Title
In vivo results using photothermal tomography for imaging cutaneous blood vessels

Authors
Choi, Bernard
Majaron, Boris
Vargas, Gracie
et al.

Publication Date
2003-07-31

DOI
10.1117/12.484140

In Vivo Results Using Photothermal Tomography for Imaging Cutaneous Blood Vessels

Bernard Choi*[a], Boris Majaron[a,b], Gracie Vargas[c], Byungjo Jung[a], Oliver Stumpp[c], Nicole M. Kang[d], Kristen M. Kelly[a], Ashley J. Welch[c], J. Stuart Nelson[a,e]

[a]Beckman Laser Institute, University of California, Irvine, CA 92612

[b]Jožef Stefan Institute, Ljubljana, Slovenia

[c]Department of Biomedical Engineering, The University of Texas, Austin, TX 78712

[d]Department of Engineering, Harvey Mudd College, Claremont, CA 91711

[e]Department of Biomedical Engineering, University of California, Irvine, CA 92697

ABSTRACT

Previous studies suggest that optimal port wine stain (PWS) laser treatment parameters require knowledge of skin characteristics such as blood vessel size, depth, and distribution. Effective and rapid imaging modalities are not widely available. In the present study, photothermal tomography (PTT) images of an *in vivo* hamster window model and human PWS skin were obtained and analyzed. Subtherapeutic laser light pulses at 585 and 600 nm were applied to skin surface and image sequences acquired with an infrared camera. A nonnegatively constrained conjugate gradient algorithm was used to reconstruct a PTT image of the initial temperature distribution immediately following pulsed laser irradiation. Vessel dimensions determined from PTT images of hamster window model skin compared well with those measured directly using video microscopy. PTT images of human PWS skin contained vessels with estimated diameters of 200-250 μm over a 250-320 μm depth range. Use of dual wavelength excitation (DWE) analysis allowed for imaging of shallow vessels.

Keywords: inverse problem; pulsed photothermal radiometry; microvasculature; vascular lesion; tomography

1. INTRODUCTION

Port wine stain (PWS) birthmarks consist of enlarged blood vessels, typically present on the face or neck. Due to high visibility of PWS, patients may experience substantial psychological

· bchoi@laser.bli.uci.edu; phone 1 949 824-9491; fax 1 949 824-6969; www.bli.uci.edu

Smart Nondestructive Evaluation and Health Monitoring of Structural and Biological Systems II, Tribikram Kundu, Editor, Proceedings of SPIE Vol. 5047 (2003) © 2003 SPIE · 0277-786X/03/$15.00

trauma. Current therapy involves use of pulsed laser light combined with cryogen spray cooling. The primary problem is that few (<10%) treated patients achieve complete removal of their PWS after multiple treatments [1]. Results of previous studies [2-7] suggest that selection of optimal treatment parameters depends on knowledge of PWS skin characteristics such as depth of the epidermal basal layer, maximum epidermal temperature rise, depth of the most superficial blood vessels, and vessel size and distribution.

Photothermal tomography (PTT) [8] is a noninvasive technique designed to provide quantitative information on the aforementioned PWS skin characteristics. Briefly, a subtherapeutic laser pulse is applied to a specified PWS area, and the subsequent increase in infrared emission is detected with a camera. A sequence of infrared images is processed with an inversion algorithm to reconstruct an image of the 3-D temperature distribution immediately following pulsed laser irradiation.

The purpose of the present study is to analyze PTT images computed from data obtained from a representative *in vivo* animal model and from a PWS subject currently undergoing treatment at the Beckman Laser Institute and Medical Clinic.

2. MATERIALS AND METHODS

2.1. PTT Theory

Telenkov et al. [8] previously provided a detailed description of PTT theory. Briefly, an infrared image sequence [$\Delta R(x,y,t>0)$] is acquired after pulsed laser irradiation. ΔR is related to the actual skin temperature distribution immediately following irradiation [$\Delta T(x,y,z,t=0)$] by the following equation:

$$\Delta R(x',y',t>0) = \iiint_{x,y,z} K(x'-x, y'-y, z, t)\,\Delta T(x,y,z,t=0)\,dx\,dy\,dz \qquad (1)$$

where K is a kernel matrix describing heat diffusion dynamics and attenuation of blackbody radiation from the skin:

$$K(x'-x,y'-y,z,t) = K_r(x'-x,y'-y,t)\cdot C\,B_\lambda'(T_0)\,\mu_{IR}\int_{z'=0}^{\infty} K_z(z'-z,t)\,e^{-\mu_{IR}z'}\,dz' \qquad (2)$$

where K_r and K_z are thermal pointspread functions in lateral and axial dimensions [9]; C is a constant accounting for numerical aperture and losses of the collection optics, and detector specifics (e.g., size, sensitivity, integration time, and detection band); $B_\lambda'(T_o)$ is the first derivative of Planck's law of radiation, evaluated at initial temperature T_o; and μ_{IR} is the attenuation coefficient of skin to blackbody radiation. Since a band limited infrared camera detection system is used, we are concerned only with μ_{IR} over the detection band. Majaron et al. [10] determined that use of a 4.5-5 μm band justifies selection of a constant μ_{IR} value (26.5 mm^{-1}).

In discrete form, Equation (1) becomes

$$\Delta \boldsymbol{R} = \boldsymbol{K} \bullet \Delta \boldsymbol{T} \tag{3}$$

where boldfaced terms denote discrete vector ($\Delta\mathbf{R}$, $\Delta\mathbf{T}$) and matrix ($\mathbf{K}$) quantities. Singular value decomposition of $\mathbf{K}$ results in a large number of extremely small singular values, demonstrating that $\mathbf{K}$ is an ill conditioned matrix [11]. Thus, a simple inversion of Equation (3) to solve for $\Delta\mathbf{T}$ is not possible. To solve Equation (3), an iterative nonnegatively constrained conjugate gradient algorithm is applied to solve for $\Delta\mathbf{T}$, given $\Delta\mathbf{R}$ and $\mathbf{K}$ [11]. The nonnegativity constraint is applied based on prior knowledge that pulsed laser heating of skin does not result in a temperature reduction below T_o.

2.2. PTT Theory – Dual Wavelength Excitation (DWE) Approach

At laser wavelengths (585 and 600 nm) we use for PTT imaging, primary absorbers in skin are epidermal melanin and hemoglobin constituents in blood. Therefore, changes in infrared emission after pulsed laser irradiation are due to light absorption by these two components. $\Delta\mathbf{R}$ measured after irradiation with 585 and 600 nm pulses can be written as follows [12]:

$$\Delta R_{585} = x + y \tag{4a}$$

$$\Delta R_{600} = \alpha x + \beta y \tag{4b}$$

where $\mathbf{x}$ and $\mathbf{y}$ are components of $\Delta\mathbf{R}$ due to blood and melanin absorption, respectively; and α and β are constants accounting for differences in light absorption in blood and melanin, respectively, at the two wavelengths. Since melanin absorption is similar at 585 and 600 nm, $\beta \approx 1$. Since blood absorption is higher at 585 than at 600 nm, $\alpha < 1$.

With appropriate selection of α and β, according to principles outlined by Majaron et al. [12, 13], PTT images of epidermal melanin and PWS blood vessels are obtained in separate reconstruction steps. Previous studies [12-14] of 1-D depth profiling of PWS skin using this dual wavelength excitation (DWE) approach have demonstrated its advantages over single wavelength excitation (SWE) (e.g., use of 585 nm alone). In the present study, we focused only on using $\mathbf{x}$ to compute PTT images of blood vessels.

2.3. Laser Parameters

A commercial pulsed dye laser (ScleroPlus™, Candela Corp., Wayland, MA) was used. This laser was capable of emitting 1.5 ms laser pulses at wavelengths of 585 and 600 nm. Subtherapeutic light doses of ~3 J/cm^2 were used in all experiments, with a laser spot diameter of ~7 mm.

2.4. Infrared Detection System

An InSb focal plane array camera (Galileo, Raytheon, Dallas, TX) imaged time resolved changes in infrared emission after pulsed laser irradiation. The nominal detection band of the camera was

3-5 μm. To obtain a uniform μ_{IR} value (see Section 2.1), a filter reduced the band to 4.5-5 μm. A unity magnification objective lens (f/2, 50 mm diameter) imaged a 1.92 × 1.92 mm area on to a 256 × 256 array of detector elements with dimensions of 30 μm × 30 μm. The high acquisition rates (700 or 1000 frames per second) required reduction of the number of active detector elements to a 64 × 64 array. Images were transferred to PC memory with a 12-bit A/D converter.

2.5. Hamster Window Model

The hamster dorsal skin flap window chamber model [15] has been used to investigation laser light interactions with microcirculation [4]. A Syrian Golden hamster was anesthetized with a 4:3 ratio mixture of ketamine and xylazine (0.1 mL/100 g body mass). The back and flanks were shaved and excess hair removed with a depilatory cream. Dorsal skin was lifted and sutured to a clamp. One complete layer of skin was removed to expose the underlying dermis and fascia of the opposing layer. A surgically implanted aluminum chamber had apertures to provide simultaneous access to the epidermal and dermal sides of the skin flap.

A color video image of the window was obtained using a CCD camera (Sony, Japan) connected to a stereo microscope (Wild, Switzerland). The animal was then positioned so the window was at the focal plane of the infrared camera. The laser handpiece was positioned perpendicular to the optical axis of the camera. A microprism in front of the camera directed laser light towards the window. A pulse of 585 nm light was applied to the window and 700 infrared images were acquired at 700 frames per second. A second image sequence was obtained after application of a 600 nm pulse to the same location. A blackbody calibration source (BB701, Omega Engineering, Stamford, CT) was used to obtain infrared emission images at various temperatures over a range 20-96°C.

2.6. PWS Subject

Infrared image sequences were acquired from an adult subject with a PWS on the left upper extremity. A region on the back of the hand was selected for imaging. Since the stratum corneum has substantially different thermal properties from epidermis and dermis, it was removed using the tape stripping technique [16]. Pads soaked with ethanol were used to remove residual adhesive and tissue fragments, and the stripped area was rehydrated with isotonic saline soaked gauze. The experimental protocol was similar to that used with the hamster window model (Section 2.5), except that 1000 images were acquired at 1000 frames per second.

2.7. Image Processing

Software written in AVS™ (Version 5, Advanced Visualization Systems, Waltham, MA), MATLAB™ (Version 6.1, The MathWorks, Natick, MA), and LabVIEW™ (Version 6i, National

Instruments, Austin, TX) was used to process infrared image sequences. Each sequence was calibrated with the blackbody images. Background temperature was subtracted from each image to obtain ΔR_{585} and ΔR_{600} sequences. DWE principles outlined by Majaron et al. [12, 13] were used to determine values of α and β. Using Equation (4), the following was derived to compute the component of ΔR_{585} and ΔR_{600} due solely to hemoglobin absorption:

$$x = \frac{\Delta R_{585} - \beta^{-1} \Delta R_{600}}{1 - \alpha\beta^{-1}} \tag{5}$$

The iterative inversion algorithm was applied to convert x to ΔT. Image volume consisted of 64 × 64 × 30 voxels, corresponding to spatial dimensions of 1.92 × 1.92 × 0.9 mm^3. Since edge artifacts were present in the images, lateral and bottom edges were cropped to obtain a 49 × 49 × 20 voxel space (1.47 × 1.47 × 0.6 mm^3). Regularization is performed by early termination [8, 11]. Prior studies [8, 17, 18] suggest the optimal number of iterations is 30-150.

3. RESULTS

Blood vessels were clearly visible from the dermal side of the hamster window model (Figure 1a). The laser spot (~7 mm diameter, Figure 1a, dashed line) covered the majority of the window. The area (3.69 mm^2) imaged with the infrared camera was considerably smaller (Figure 1a, solid line; Figure 1b). A large vertical blood vessel (~250 μm diameter) was present along the right edge of the area. Two smaller angled vessels (~50 and 150 μm diameters) were present in the lower right corner.

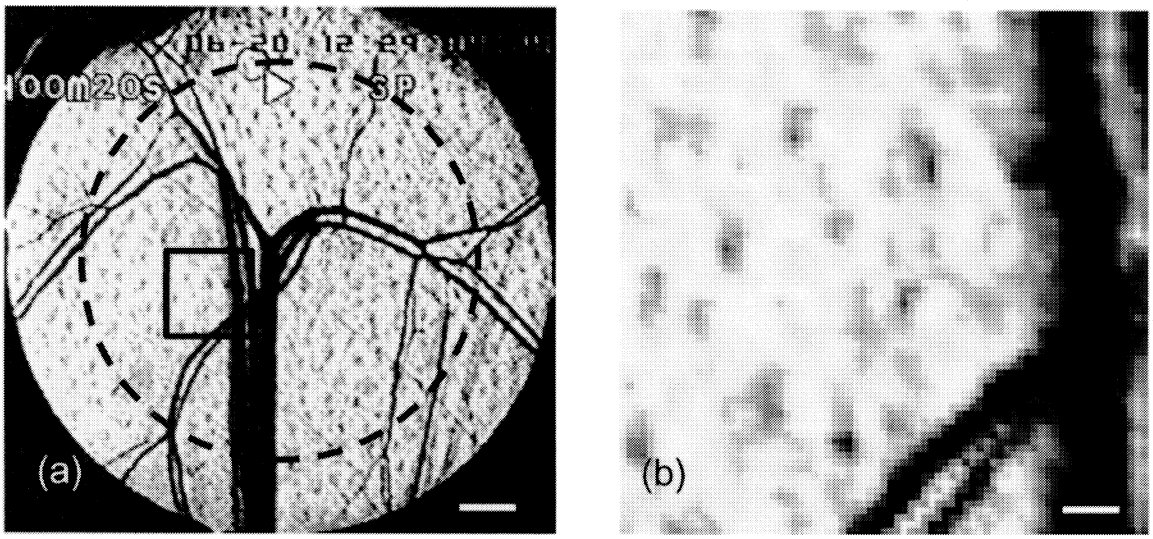

Figure 1. Digital image of 1 cm diameter hamster window model from the subdermal side. Blood vessels are clearly visible. (a) Entire window. The dashed line outlines the area covered by the laser spot diameter (~7 mm). The solid line outlines the smaller area imaged with the infrared camera. Scale bar = 1 mm. (b) Close up view of area imaged with the infrared camera. Diameter of the large vertical blood vessel was ~250 μm. Scale bar = 250 μm.

After pulsed laser irradiation of the window at 585 and 600 nm, infrared image sequences were acquired at 700 frames per second. Since infrared images were acquired from the opposing epidermal side of the window, the video and infrared images are mirror images of each other. Thus, the infrared images in Figure 2 were "flipped" laterally to correspond to the geometry shown in Figure 1. In the 585 nm image sequence (Figure 2), focal points of heating were evident in early images (Figure 2b). At 100 ms after laser irradiation, a high emission region along the right edge was evident (Figure 2c). At 250 ms, this region was broader, and a second region of increased emission was evident in the lower right corner (Figure 2d, arrow).

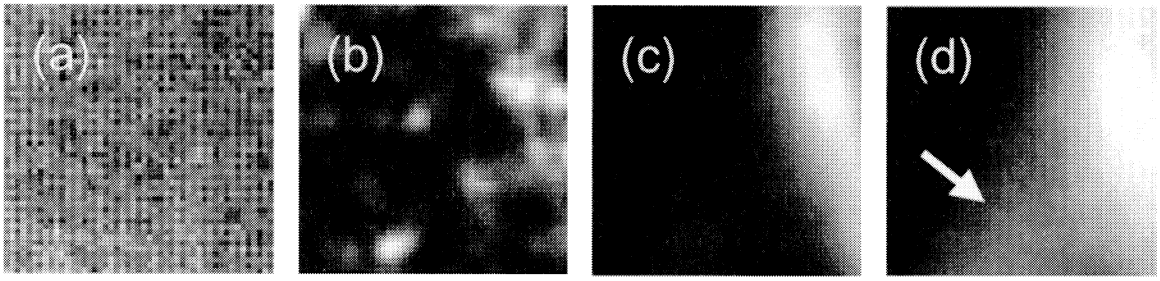

Figure 2. Four infrared images acquired from the area shown in Figure 1b. (a) Before laser irradiation, (b) 10 ms after pulsed laser irradiation (λ = 585 nm, pulse duration = 1.5 ms), and (c) 100 ms and (d) 250 ms after the end of the pulse. In (c), increased infrared emission due to blood vessel heating was evident. In (d), features of a second region of heating (arrow) were evident.

In depth resolved *en face* cross sections (Figure 2) of a DWE PTT image reconstructed from the infrared image sequence, the vertical vessel was evident at a depth of 165 μm (Figure 3a). Note that a full scale contrast stretch was applied to each section to use the entire 8 bit grayscale dynamic range for image display. From this section, the vessel diameter was estimated to be ~300 μm. At a depth of 255 μm, features of a single ~200 μm diameter angled vessel are evident (arrow, Figure 3b).

En face cross sections of a SWE PTT image reconstructed from an infrared image sequence taken from PWS skin did not reveal features of subsurface blood vessels (Figure 4(a-d)). In the surface section (Figure 4a), epidermal melanin heating was evident. However, in deeper sections (Figures 4(b-d)), no vessels were evident. In sections of a DWE PTT image reconstructed from image sequences acquired at the same location, three blood vessels are evident at depths of 255-315 μm (Figure 5). Vessel diameters were estimated at 200-250 μm. In the surface section (Figure 5a), no evidence of epidermal heating was evident.

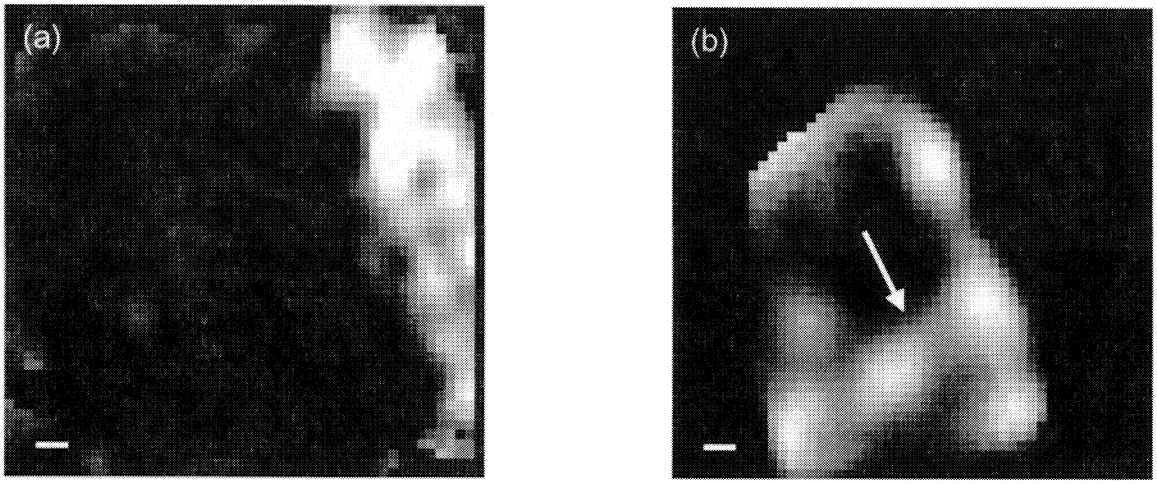

Figure 3. *En face* cross sections of DWE PTT image reconstructed from infrared image sequences acquired from the hamster window model area shown in Figure 1b. Depths of (a) 165 μm and (b) 255 μm are shown. In (a) the vertical vessel diameter is ~300 μm. In (b) the angled vessel (arrow) diameter is ~200 μm. A full scale contrast stretch was applied to each image to maximize use of the 8 bit grayscale dynamic range. Scale bar = 100 μm.

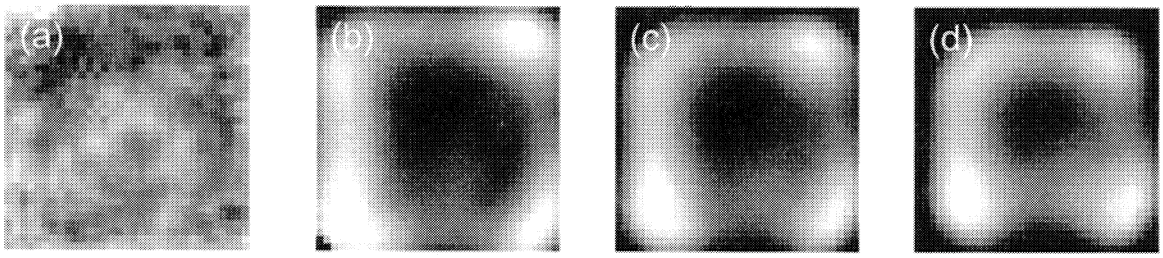

Figure 4. *En face* cross sections of SWE PTT image reconstructed from an infrared image sequence acquired from PWS skin. Section depths are (a) 15, (b) 255, (c) 285, and (d) 315 μm. In (a), melanin heating is evident. In (b-d), blood vessel structure is not apparent. A full scale contrast stretch was applied to each image to maximize use of the 8 bit grayscale dynamic range. Section size is 1 mm × 1 mm.

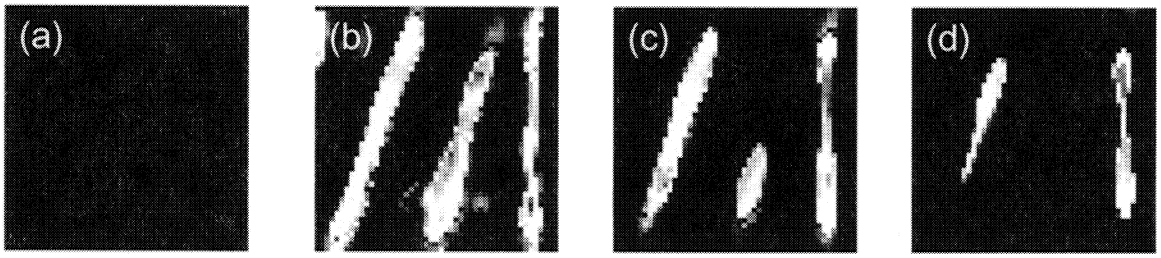

Figure 5. *En face* cross sections of DWE PTT image reconstructed from infrared image sequences acquired from PWS skin. Section depths are (a) 15, (b) 255, (c) 285, and (d) 315 μm. In (a), melanin heating is not evident. In (b-d), three blood vessels are apparent. Vessel diameters are estimated at approximately 200-250 μm. A full scale contrast stretch was applied to each image to maximize use of the 8 bit grayscale dynamic range. Section size is 1.47 mm × 1.47 mm.

A 3-D isothermal rendering of SWE (Figure 6a) and DWE (Figure 6b) PTT images of the data shown in Figures 4-5 further illustrates the differences between the two approaches. Epidermal melanin heating was evident in the SWE PTT image but absent in the DWE PTT image. Blood vessels were absent and present in the SWE and DWE PTT images, respectively. Isotherms were $\Delta T = 10°C$ and 40°C, respectively.

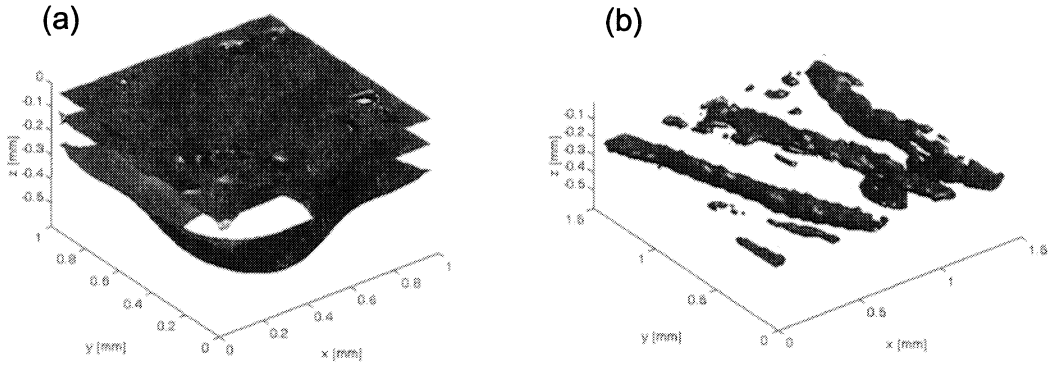

Figure 6. 3-D isothermal renderings of (a) SWE and (b) DWE PTT images of PWS skin. Isotherms are $\Delta T = 10°C$ and 40°C, respectively.

4. DISCUSSION

Laser PWS therapy can be improved with knowledge of skin characteristics, such as depth of the epidermal basal layer, maximum epidermal temperature rise, depth of the most superficial blood vessels, and vessel size and distribution. Previous studies [12-14] have shown that 1-D DWE depth profiling of PWS skin provides information on all these parameters except for vessel size and distribution. Telenkov et al. [8] have demonstrated the potential of SWE PTT for imaging blood vessels in an *in vivo* chick chorioallantoic membrane (CAM) model and PWS skin. While the CAM serves as an appropriate model for evaluating the fidelity of PTT images, the model does not include epidermal light absorption and skin light scattering, which may alter substantially overall heating patterns in the microvasculature.

The hamster window model (Figure 1) has been used previously for investigating light interactions with blood vessels [4]. Since a full thickness of skin remains intact after surgery, epidermal light absorption and light scattering are included in PTT imaging studies. By changing location of the infrared imaging area, multiple images can be obtained from the same window. Vessel diameters can be measured directly from microscopic video images and compared with lateral vessel dimensions determined from PTT images.

In infrared images acquired soon after subtherapeutic laser irradiation (Figure 2b), focal regions of heating are visible. These probably coincide with dense regions of melanin located at the epidermal basal layer. At later times, regions of high infrared emission are due primarily to light

absorption in dermal blood vessels. Initially, a region of heating along the right edge is visible (Figure 2c), coinciding with the vertical blood vessel shown in Figure 1b. At later times, an angled region of heating is visible in the lower right of the infrared emission image (Figure 2d), which is due to light absorption in the two angled vessels shown in Figure 1b. Thus, from cursory analysis of infrared image sequences, it is possible to determine relative depths of vessels.

En face cross sections of a DWE PTT image computed using this image sequence showed features of the vertical vessel and one angled vessel (Figure 3). The ~300 μm vertical vessel diameter estimated from the heating pattern visible in the section corresponds well with the "true" 250 μm diameter measured in the video image (Figure 1b), thereby demonstrating the potential of PTT as an imaging modality for PWS skin. The presence of only one angled vessel in the PTT image is probably due to the ~10-20 μm spacing between the two angled vessels apparent in Figure 1b. Best-case lateral spatial resolution of our system (~30 μm) is insufficient to identify correctly the presence of two distinct vessels. In reality, spatial resolution of imaging techniques similar to PTT is known to degrade with increasing depth [19]. However, we are encouraged by the favorable comparison between the estimated angled vessel diameter (~200 μm) and the sum of the actual vessel diameters (~200 μm).

Vessel diameters from PTT images were measured using lateral dimensions of the heated region in the *en face* sections. From preliminary modeling data by Smithies et al. [17, 20], vessel diameters determined from PTT images matched well with the actual diameters when the FWHM temperature rise of the vessels was used to define radial vessel boundaries. Further use of this hamster window model in conjunction with numerical simulations [17] will allow us to evaluate the validity of this assumption, and accuracy and limitations of PTT for determining accurately PWS vessel diameters.

In PTT images, blood vessel isotherms are not cylindrical in shape, but have local regions of constriction and dilation. Unfortunately, determination of an average vessel diameter is not a trivial task. Sophisticated image processing techniques are required to determine vessel cross sectional vessel at multiple lateral positions. A low pass filter based template matching scheme [21] will be investigated as a potential tool for outlining vessel boundaries and determining more precisely vessel dimensions in PTT images.

In the present study, 100 iterations of the inversion algorithm were performed to compute PTT images. In prior studies [8, 17, 20], 30-75 iterations were used. As a first step, we used 100 iterations based on preliminary 3-D DWE imaging results [18]. Theoretical modeling and hamster window studies will be used to investigate the role of iteration number on PTT image accuracy.

We are involved in an ongoing clinical study to acquire infrared image sequences from PWS subjects. In the present study, two PTT image examples (Figures 4 and 5) of the same site are presented. Telenkov et al. [8] demonstrated that SWE PTT can image PWS skin. In the present study, the reconstructed SWE PTT image (Figures 4 and 6a) did not provide information on blood vessel characteristics. However, with DWE analysis, the reconstructed PTT image (Figures 5 and 6b) showed the presence of three blood vessels. From 1-D DWE depth profiling analysis (not shown here) of the same site, the average epidermal basal layer depth was ~200 μm. Since the most superficial vessel (255 μm depth) was in close proximity to the basal layer, the SWE approach was limited in its ability to differentiate heating of superficial vessels from that of the lower epidermal regions [12]. Use of the DWE approach (Equation 5) allows us to image selectively the vascular component of PWS skin, as evidenced by absence of epidermal heating in the superficial cross section (Figure 5a). To validate these measurements, future studies are planned to correlate vessel diameters and depths determined from PTT images with those identified using optical Doppler tomography [22] and histological analysis of biopsies [23].

5. CONCLUSIONS

Blood vessel dimensions and lateral position determined from PTT images of hamster window model skin compared well with those measured directly from microscopic video images. PTT images of human PWS skin contained vessels with estimated diameters of 200-250 μm over a 250-320 μm depth range. Use of dual wavelength excitation (DWE) analysis allowed for imaging of shallow vessels.

ACKNOWLEDGMENTS

Funding sources include the Arnold and Mabel Beckman Fellows Program (BC); National Institutes of Health (NIH) (AR-43419 and GM-62177); Slovenian Ministry of Education and Science (BM); Dermatology Foundation and American Society for Lasers in Medicine and Surgery (KMK); and institutional support from the Air Force Office of Scientific Research, NIH, and the Beckman Laser Institute and Medical Clinic Endowment.

REFERENCES

1. Svaasand LO, van Gemert MJC, Verkruysse W, Fiskerstrand EJ, and Norvang LT, "Dosimetry for laser treatment of port wine stains," in *Laser-Tissue Interaction X*, Jacques SL, Mueller GJ, Roggan A, Sliney DH, Eds., *Proceedings SPIE* **3601**, 463-471 (1999).

2. van Gemert MJC, Nelson JS, Milner TE, Smithies DJ, Verkruysse W, de Boer JF, Lucassen GW, Goodman DM, Tanenbaum BS, Norvang LT, and Svaasand LO, "Non-invasive determination of port wine stain anatomy and physiology for optimal laser treatment strategies," *Phys Med Biol* **42**, 937-950 (1997).

3. de Boer JF, Lucassen GW, Verkruysse W, and van Gemert MJC, "Thermolysis of port-wine-stain blood vessels: Diameter of a damaged blood vessel depends on the laser pulse length," *Laser Med Sci* **11,** 177-180 (1996).

4. Barton JK, Vargas G, Pfefer TJ, and Welch AJ, "Laser fluence for permanent damage of cutaneous blood vessels," *Photochem Photobiol* **70,** 916-920 (1999).

5. Svaasand LO, Fiskerstrand EJ, Kopstad G, Norvang LT, Svaasand EK, Nelson JS, and Berns MW, "Therapeutic response during pulsed laser treatment of port-wine stains: Dependence on vessel diameter and depth in dermis," *Laser Med Sci* **10,** 235-243 (1995).

6. Kimel S, Svaasand LO, Cao D, Hammer-Wilson MJ, and Nelson JS, "Vascular response to laser photothermolysis as a function of pulse duration, vessel type, and diameter: Implications for port wine stain laser therapy," *Laser Surg Med* **30,** 160-169 (2002).

7. Verkruysse W, Majaron B, Tanenbaum BS, and Nelson JS, "Optimal cryogen spray cooling parameters for pulsed laser treatment of port wine stains," *Laser Surg Med* **27,** 165-170 (2000).

8. Telenkov SA, Tanenbaum BS, Goodman DM, Nelson JS, and Milner TE, "In vivo infrared tomographic imaging of laser-heated blood vessels," *IEEE J Sel Top Quant Elect* **5,** 1193-1199 (1999).

9. Carslaw HS and JC Jaeger, *Conduction of Heat in Solids*, Clarendon Press, Oxford (1959).

10. Majaron B, Verkruysse W, Tanenbaum BS, Milner TE, and Nelson JS, "Spectral variation of the infrared absorption coefficient in pulsed photothermal profiling of biological samples," *Phys Med Biol* **47,** 1929-1946 (2002).

11. Milner TE, Goodman DM, Tanenbaum BS, and Nelson JS, "Depth profiling of laser-heated chromophores in biological tissues by pulsed photothermal radiometry," *J Opt Soc Am A* **12,** 1479-1488 (1995).

12. Majaron B, Verkruysse W, Tanenbaum BS, Milner TE, Telenkov SA, Goodman DM, and Nelson JS, "Combining two excitation wavelengths for pulsed photothermal profiling of hypervascular lesions in human skin," *Phys Med Biol* **45,** 1913-1922 (2000).

13. Majaron B, Milner TE, and Nelson JS, "Determination of parameter β for dual-wavelength pulsed photothermal profiling of human skin," *Rev Sci Instrum* **74,** 387-389 (2003).

14. Choi B, Majaron B, and Nelson JS, "Theoretical evaluation of pulsed photothermal radiometry (PPTR) for depth profiling of PWS skin," *Proceedings SPIE* (2003, in press).

15. Papenfuss HD, Gross JF, Intaglietta M, and Treese FA, "A transparent access chamber for the rat dorsal skin fold," *Microvasc Res* **18,** 311-318 (1979).

16. Bommannan D, Potts RO, and Guy RH, "Examination of stratum corneum barrier function in vivo by infrared spectroscopy," *J Invest Dermatol* **95,** 403-408 (1990).

17. Smithies DJ, Milner TE, Nelson JS, and Goodman DM, "Solution of the infrared tomography inverse problem," in *Laser-Tissue Interaction VII*, Jacques SL, Ed., *Proceedings SPIE* **2681**, 2-4 (1996).

18. Majaron B, Milner TE, and Nelson JS, "Pulsed photothermal imaging of port-wine stain birthmarks using two laser wavelengths," *Laser Surg Med* **Suppl 14,** 8 (2002).

19. Power JF, "Inverse problem theory in the optical depth profilometry of thin films," *Rev Sci Instrum* **73,** 4057-4141 (2002).

20. Smithies DJ, van Gemert MJC, Hansen MK, Milner TE, and Nelson JS, "Three-dimensional reconstruction of port wine stain vascular anatomy from serial histological sections," *Phys Med Biol* **42,** 1843-1847 (1997).

21. Sukanya P, Takamatsu R, and Sato M, "The surface-shape operator and multiscale approach for image classification," *IEICE T Fund Elect* **E81A,** 1683-1689 (1998).

22. Chen Z, Zhao Y, Srinivas SM, Nelson JS, Prakash N, and Frostig RD, "Optical Doppler tomography," *IEEE J Sel Top Quant Elect* **5,** 1134-1142 (1999).

23. Milner TE, Smithies DJ, Goodman DM, Lau A, and Nelson JS, "Depth determination of chromophores in human skin by pulsed photothermal radiometry," *Appl Optics* **35,** 3379-3385 (1996).